Національна академія наук України

ІНСТИТУТ ФІЗИКИ КОНДЕНСОВАНИХ СИСТЕМ ім. І.Р. ЮХНОВСЬКОГО

ICMP–26–03E

T.Hutak, J.Richter, H.-J.Schmidt, J.Schnack,
T.Krokhmalskii, O.Derzhko

THERMODYNAMICS OF THE SPIN-S HEISENBERG ANTIFERROMAGNET ON THE KAGOME LATTICE: FINITE-SIZE NUMERICS AND HIGH-TEMPERATURE SERIES EXPANSION

ЛЬВІВ

УДК: 537.9; 537.622

PACS: 75.10.-b

Термодинаміка спін-S Гайзенбергового антиферомагнетика на гратці кагоме: числові дані для скінченнорозмірних систем і розвинення у високотемпературні ряди

Т.Гутак, Й.Ріхтер, Г.-Ю.Шмідт, Ю.Шнак, Т.Крохмальський, О.Держко

Анотація. Ми досліджуємо термодинамічні величини для квантового Гайзенбергового антиферомагнетика зі спіном $S > 1/2$. Для цього ми використовуємо метод точної діагоналізації і метод Ланцоша при скінченних температурах для скінченнорозмірних систем, а також високотемпературні розвинення до 11 порядку за $\beta = 1/T$ і метод ентропії. Ми зосереджуємося на температурних профілях ентропії, теплоємності та сприйнятливості. Зокрема, ми обговорюємо як температурна залежність теплоємності $c(T)$ змінюється, коли квантове число спіна S росте до класичної границі $S \to \infty$.

Thermodynamics of the spin-S Heisenberg antiferromagnet on the kagome lattice: Finite-size numerics and high-temperature series expansion

T.Hutak, J.Richter, H.-J.Schmidt, J.Schnack, T.Krokhmalskii, O.Derzhko

Abstract. We examine thermodynamic quantities for the kagome-lattice Heisenberg antiferromagnet with spin $S > 1/2$. To this end, we use exact diagonalization and finite-temperature Lanczos method data for finite systems as well as high-temperature series expansion up to order 11 in $\beta = 1/T$ and the entropy method. We focus on the temperature profiles of entropy, specific heat, and susceptibility. In particular, we discuss how the temperature dependence of the specific heat $c(T)$ varies as the spin quantum number S grows to the classical limit $S \to \infty$.

© Інститут фізики конденсованих систем ім. І.Р. Юхновського 2026
Yukhnovskii Institute for Condensed Matter Physics 2026

Препринти Інституту фізики конденсованих систем імені І.Р. Юхновського НАН України доступні на WWW-сервері інституту за адресою https://icmp.lviv.ua/

The preprints of the Yukhnovskii Institute for Condensed Matter Physics of the National Academy of Sciences of Ukraine are available from Institute's WWW server (https://icmp.lviv.ua/en)

Тарас Ігорович Гутак
Йоганес Ріхтер
Гайнц-Юрген Шмідт
Юрген Шнак
Тарас Євстахійович Крохмальський
Олег Володимирович Держко

Термодинаміка спін-S Гайзенбергового антиферомагнетика на гратці кагоме: числові дані для скінченнорозмірних систем і розвинення у високотемпературні ряди

Роботу отримано 18 вересня 2026 р.

Затверджено до друку Вченою радою ІФКС ім. І.Р. Юхновського НАН України

Рекомендовано до друку відділом квантової статистики

Виготовлено при ІФКС ім. І.Р. Юхновського НАН України
© Усі права застережені

1. Introduction

The spin-S Heisenberg model with antiferromagnetic nearest-neighbor exchange coupling J on the kagome lattice (KHAF) is a paradigmatic model in frustrated quantum magnetism, which attracts a lot of attention both from theoretical and experimental sides [1–3]. The spin value $S = 1/2$ represents the pure quantum case, whereas $S \to \infty$ corresponds to the classical one. Thus, the spin value S controls the role of quantum fluctuations which together with geometrical frustration and thermal fluctuations are known to produce intriguing properties of such a spin-lattice system. In what follows, we illustrate how some temperature characteristics of the KHAF depend on S using two complementary techniques. Prior to that we briefly recall what is needed for our study.

There are plenty of papers concerning the ground-state properties of the KHAF. It is commonly accepted that the ground state of the $S = 1/2$ KHAF is a gapless spin liquid, although, there are several possible spin-liquid candidates, and the precise nature of the ground state is still under debate, see Refs. [4–7]. Various proposals have been suggested and examined for the ground state of the $S = 1$ KHAF [8–23]. Although nonmagnetic, these proposals favor a valence-bond crystal order. Among them are a hexagon-singlet solid state [8], a resonating Affleck-Kennedy-Lieb-Tasaki loop state [12], or a simplex valence-bond crystal order favoring trimerization [10, 13, 14, 16]. The ground-state energy per site e_0 calculated by various methods can be found in Appendix A. Most of the data lie within or close to the interval $[-1.41, -1.40]$ with $J = 1$ being the energy scale. Furthermore, the $S = 1$ KHAF is expected to be gapped, and the nonmagnetic excitations have a finite energy gap comparable to the one for the magnetic excitations. The value of the spin gap is estimated in the range $0.2 - 0.3$ [16]. The density-matrix renormalization group calculations of Ref. [19] give the following estimates for the singlet-triplet gap: $\Delta_{s-t} = 0.178 \pm 0.005$ for the hexagon-singlet solid state and $\Delta_{s-t} = 0.279\,7$ for the triangular valence-bond solid state. For $S \geq 3/2$ a ground-state magnetic long-range order is expected to appear [11, 15, 21, 24]. It was argued that the $\sqrt{3} \times \sqrt{3}$ state is the ground state which, as always, melts at any non-zero temperature [24]. The ground-state energy for the $S = 3/2$ KHAF can be found in Appendix A. Finally, the classical ground states ($S \to \infty$) were discussed in Refs. [25, 26]. The set of all ground states is disordered, but as $T \to 0$, the entropy of fluctuations selects nematic correlations.

Capturing thermodynamic behavior of the KHAF in the whole temperature range is a hard problem. Thus, for the $S = 1/2$ KHAF an

extra low-temperature peak or shoulder in the magnetic specific heat at the temperature about ten times smaller than J is debated [27–37]. Besides, an enhanced magnetic susceptibility at low temperatures below half of J was observed [35, 38]. Finite-temperature properties of the $S = 1$ KHAF have been examined very recently in Ref. [23] using the finite-temperature Lanczos method. The most characteristic feature observed there is a double-peak structure of the specific heat $c(T)$ for all considered cluster sizes, $N = 21$, 24, and 27. The magnetic susceptibility exhibits a broad maximum around $T/J \approx 0.4$ and then decreases rapidly at low temperatures. For the $S = 3/2$ KHAF, the specific heat exhibits a T^2 behavior and the susceptibility approaches a finite constant as $T \to 0$ [24]. Finally, for the classical case $S \to \infty$, it is known that the specific heat with temperature decrease exhibits a maximum before it assumes the value 11/12 at $T = 0$ [25], whereas the susceptibility reaches the value $\chi_0 = 1/6$ at $T = 0$ [39, 40].

Concerning experiments, high quality crystals of herbertsmithite $ZnCu_3(OH)_6Cl_2$, in which the copper ions carrying spin one-half sit on a kagome lattice, were synthesized in 2005 [41]. Many more $S = 1/2$ KHAF realistic materials are known nowadays. This stimulates an interest in theoretical studies of the thermodynamics of the $S = 1/2$ KHAF. It would be highly desirable to compare experiments with theory [41–46]. However, for a precise explanation of finite-temperature measurements it is necessary to explore side effects unavoidably present in real crystals, see, e.g., Ref. [37]. Although, various magnetic kagome compounds with $S > 1/2$ exist, see, e.g., Refs. [47–58] for the $S = 1$ case and Refs. [59–63] for the $S > 1$ case, there are only few theoretical papers on the finite-temperature properties of the corresponding KHAFs [23, 24, 64]. Let us also note that an effective low-energy theory of some $S = 1/2$ Heisenberg systems may be related to the $S = 1$ KHAF [65, 66] that provides yet another motivation for investigations of the thermodynamics of the $S > 1/2$ KHAF.

In the present paper, we study the thermodynamics of the spin-S KHAF, $S > 1/2$, focusing on the entropy $s(T)$, the specific heat $c(T)$, and the susceptibility $\chi(T)$. Theoretical methods to study the thermodynamics of highly frustrated quantum Heisenberg antiferromagnets are rather limited. Quantum Monte Carlo simulations are inapplicable because of the sign problem, exact diagonalization and finite-temperature Lanczos methods are limited to relatively small system sizes N [35, 67, 68], which become even smaller when $S > 1/2$ since the Hilbert space dimension grows as $(2S+1)^N$, the numerical linked-cluster approach to quantum lattice models cannot access sufficiently low temperatures [32, 33],

whereas the second-order rotation-invariant Green's-function method is too crude to reveal fine low-temperature features [64]. Furthermore, a raw high-temperature expansion being complemented by Padé approximants is restricted to the temperature range above $T/J \sim 0.5$. Here, we use as a main approach the entropy-method interpolation of high-temperature expansion, Refs. [31, 69, 70]. The key element of the entropy method is a clever procedure of interpolation between the known low- and high-temperature properties in the microcanonical ensemble which respects the sum rules constraining the specific heat [26, 31, 37, 69–76]. In addition to the entropy-method treatment, we perform numerical calculations for finite-size systems up to $N = 21$ for $S = 1$ and up to $N = 18$ for $S = 3/2$. Our aim is to follow how the thermodynamic properties vary as the spin value S increases from the pure quantum limit $S = 1/2$ to the classical limit $S \to \infty$.

We conclude this section with introducing the model and notations. We consider the kagome-lattice Heisenberg antiferromagnet with the Hamiltonian

$$H = J \sum_{\langle nm \rangle} \boldsymbol{S}_n \cdot \boldsymbol{S}_m. \tag{1}$$

Here, the antiferromagnetic exchange coupling $J > 0$ is set to unity, $J = 1$, the sum runs over nearest-neighbor bonds on the kagome lattice, and $\boldsymbol{S}_n^2 = S(S+1)$, $S = 1/2, 1, 3/2, \ldots$ (in what follows, the largest considered value of S is 4). We set $\hbar = 1$ and $k_B = 1$ throughout the paper.

In the rest of the paper, we first concisely explain the exploited methods (Section 2) and then report the obtained results (Section 3). We close with a brief summary (Section 4). Two appendices contain some source information for the spin-S KHAF as well as a comparative study of the spin-S square-lattice Heisenberg antiferromagnet.

2. Methods

2.1. Finite-temperature Lanczos method

The first approach of our study is the exact diagonalization and the finite-temperature Lanczos methods which allow to illustrate low-lying energy levels and temperature dependences $s(T)$, $c(T)$, and $\chi(T)$ for the finite-size $S = 1$ and $S = 3/2$ KHAF. To this end, we use clusters with $N = 15$ ($S = 3/2$), $N = 18$ ($S = 1$, 3/2), and $N = 21$ ($S = 1$) with periodic boundary conditions imposed.

The finite-temperature Lanczos method (FTLM) is explained in some detail in Refs. [23, 35, 77]. The key element is the approximation of the canonical ensemble average using a Monte-Carlo like representation for it, i.e., the sum over a complete set of $(2S+1)^N$ basis vectors inherent in the average is replaced by a much smaller sum over R random vectors $|\nu\rangle$ for each symmetry-related subspace $\mathcal{H}(\gamma)$ of the Hilbert space, where except the conservation of total $\mathcal{S}^z = \sum_{n=1}^{N} S_n^z$ we also use the lattice symmetries of the Hamiltonian to decompose the full Hilbert space into mutually orthogonal subspaces labeled by γ. We denote by N_γ the dimension of the γ subspace, $N_\gamma = \dim[\mathcal{H}(\gamma)]$. For each γ, the exponential of the Hamiltonian is then approximated by its spectral representation in a Krylov space spanned by the N_L Lanczos vectors starting from the respective random vector $|\nu\rangle$. As a result, the FTLM representation of the average reads:

$$\langle(\ldots)\rangle = \frac{1}{Z}\sum_{\gamma=1}^{\Gamma}\frac{N_\gamma}{R}\sum_{\nu=1}^{R}\sum_{n=1}^{N_L} e^{-\frac{\epsilon_n^{(\nu)}}{T}}\,|\langle n(\nu)|\nu\rangle|^2\,(\ldots)_n^{(\nu)},$$
$$Z = \sum_{\gamma=1}^{\Gamma}\frac{N_\gamma}{R}\sum_{\nu=1}^{R}\sum_{n=1}^{N_L} e^{-\frac{\epsilon_n^{(\nu)}}{T}}\,|\langle n(\nu)|\nu\rangle|^2\,. \qquad (2)$$

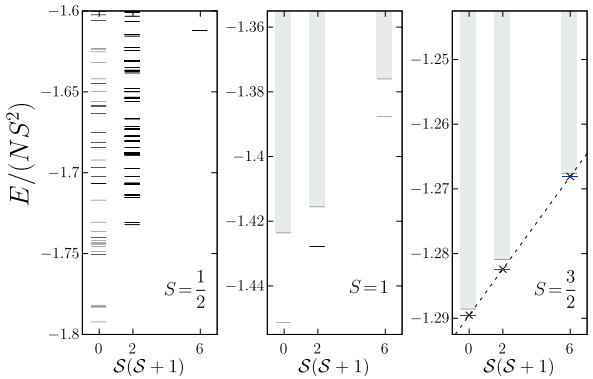


Figure 1. Low-lying energy levels E versus total spin squared $(\sum_{n=1}^{N}\boldsymbol{S}_n)^2 = \mathcal{S}(\mathcal{S}+1)$ of the $N=18$ KHAF for (left) $S=1/2$, (middle) $S=1$, and (right) $S=3/2$. Note that for $S=1/2$ we present the exact spectrum, whereas for $S>1/2$ only the Lanczos spectrum (regions of higher-energy levels are denoted as gray stripes). For $S=3/2$ (right panel), the quasi-degenerate joint states in the subspaces with $\mathcal{S}=0,1,$ and 2 are colored in red, green, and blue, respectively.

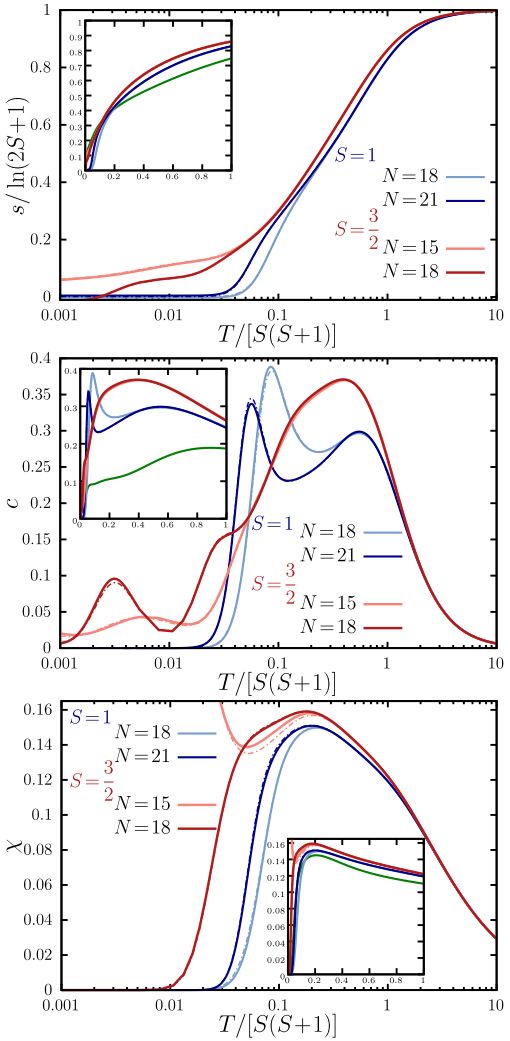


Figure 2. Numerics for (top) $s(T)$, (middle) $c(T)$, and (bottom) $\chi(T)$ of the $S=1$ ($N=18,21$) and $S=3/2$ ($N=15,18$) KHAF. For $S=1$, solid lines correspond to $R=200$ ($N=18$), $R=50$ ($N=21$), dash-dotted lines correspond to $R=100$ ($N=18$), $R=10$ ($N=21$); for $S=3/2$, solid lines correspond to $R=40$ ($N=15$), $R=20$ ($N=18$), dash-dotted lines correspond to $R=20$ ($N=15$), $R=16$ ($N=18$), see Sec. 2.1. The insets present the same data in linear scale; besides, they contain results for the $S=1/2$ KHAF ($N=36$, green) for reference.

Here, $|n(\nu)\rangle$ is the nth eigenvector of H in the Krylov space with the corresponding energy $\epsilon_n^{(\nu)}$, whereas Z is the canonical partition function.

Figures 1 and 2 present our finite-size FTLM results. The former figure reports the energy spectra (actually, pseudospectra of Lanczos energies for $S = 1, 3/2$) in the subspaces with low total $\mathcal{S} = 0, 1, 2$. The latter figure reports the thermodynamic quantities (entropy, specific heat, and susceptibility).

With respect to low-energy spectra, we have to recall that a careful analysis of exact-diagonalization data on small clusters may give hints concerning long-range ordering (or not) in the thermodynamic limit [78, 79]. This was demonstrated for the $S = 1/2$ Heisenberg antiferromagnet on the triangular lattice [80–83] and the kagome lattice [84–86]. Having only very few accessible KHAF clusters investigated by FTLM, we cannot perform a similar analysis for the $S > 1/2$ cases. On the other hand, the nature of the ground state is not in the focus of our study: We only use the knowledge concerning this issue available in literature. But, as discussed below, our low-energy spectrum data agree with the existing suppositions.

2.2. High-temperature expansion and entropy method

The main method of our investigation is the high-temperature expansion (HTE) augmented further by the entropy-method interpolation which was elaborated for thermodynamically large spin systems without a finite-temperature phase transition in Refs. [31, 37, 69, 70]. First, we use the Magdeburg HTE code of Refs. [87, 88] [1], in an extended version up to nth order ($n = 13$ for $S = 1/2$ and $n = 11$ for $S > 1/2$) [2]. Thus, we compute the series of the specific heat (per site) $c(T) = \sum_{i=2}^{n} d_i\beta^i + \mathcal{O}(\beta^{n+1})$ ($d_1 = 0$) and the static uniform susceptibility (per site) $\chi(T) = \sum_{i=1}^{n} c_i\beta^i + \mathcal{O}(\beta^{n+1})$ with respect to the inverse temperature $\beta = 1/T$. As a result, we have the following high-temperature series for the Helmholtz free energy (per site) for low magnetic fields h ($g\mu_B = 1$)

$$-\beta f(T,h) = \frac{\ln Z(\beta,h,N)}{N}$$

[1] It is freely available at `http://www.uni-magdeburg.de/jschulen/HTE/`.

[2] Recently, an algorithm for calculating high-temperature expansion series of Heisenberg models in the thermodynamic limit, which accounts for the presence of a magnetic field, has been reported [89]; however, this algorithm is restricted to the spin value $S = 1/2$.

$$\stackrel{\beta\to 0}{=} \ln(2S+1) + \sum_{i=2}^{n} \frac{d_i}{(i-1)i}\beta^i + \mathcal{O}(\beta^{n+1}) + \frac{1}{2}\beta\left(\sum_{i=1}^{n} c_i\beta^i + \mathcal{O}(\beta^{n+1})\right)h^2 + \mathcal{O}(h^4), \quad (3)$$

where $Z(\beta,h,N)$ is the canonical partition function. HTE up to 10th order for arbitrary spin S can be found in Appendix B of Ref. [88]. In the present paper, we use one more order: The coefficients d_{11} and c_{11} for $S = 1$, 3/2, 2, 5/2, 3, 7/2, and 4 can be found in Appendix A.

The most straightforward way to extend the region of validity of the raw HTE is to construct simple Padé approximants [88], which are rational functions where the numerator is a polynomial in β of degree u and the denominator one of degree d. Our studies on the spin-S KHAF used HTE up to 11th order. Therefore, we may construct $[u,d](T)$, $u + d \le n = 11$, and in what follows we show the close to diagonal Padé approximants for $n = 10$ and $n = 11$: $[4,6](T)$, $[5,5](T)$, $[6,4](T)$ and $[5,6](T)$, $[6,5](T)$.

However, as a key tool, we exploit the entropy method [31, 37, 69, 70] to interpolate between the high-temperature behavior given by the HTE and the presumed low-temperature behavior this way obtaining thermodynamic quantities over the full temperature range. In a nutshell, we work in the microcanonical ensemble with the entropy (per site) as a function of the internal energy (per site) $s(e)$. We need, besides the known Maclaurin series for $s(e)$ up to order $n = 11$, the ground-state energy per site e_0 and the behavior of the specific heat $c(T)$ as $T \to 0$ (either like AT^α or $\propto e^{-\Delta/T}$), which determines $s(e)$ as $e \to e_0$. Then we interpolate an auxiliary function $G(e)$, which depends on the specific low-temperature behavior of $c(T)$ and is uniquely related to $s(e)$, using Padé approximants $[u,d](e)$, $u+d \le n = 11$. Interestingly, the entropy method gives the values of A or Δ. According to Ref. [37], if e_0 is exact, the adopted low-temperature $c(T)$ is correct, and n is sufficiently large, the approximate entropy-method specific heat $c_{\rm app}(T)$ for all $[u,d](e)$ is close to the exact one [3]. The described prescription can be straightforwardly extended in the presence of a magnetic field to obtain the susceptibility $\chi(T)$, however, $\chi_0 \equiv \chi(T{=}0)$ is necessary as an extra input parameter if the low-energy excitations are gapless. We are not aware of calculations of χ_0 for $S > 1$ besides the rotation-invariant Green's-function method data [64] which, however, are not accurate enough to be used for interpolation.

[3] This observation can be used to proceed even in the case when the ground state and low-energy excitations are unknown [37, 72, 73, 75].

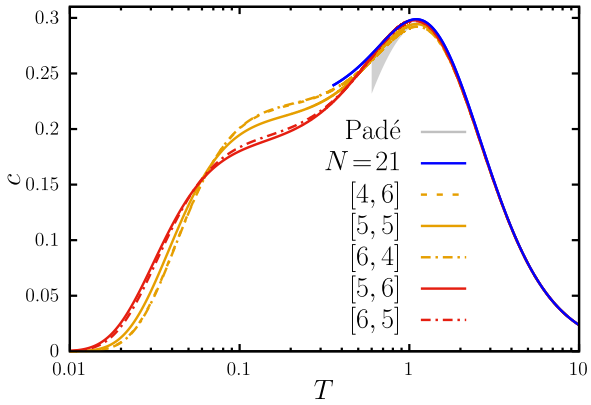


Figure 3. Entropy-method results (orange and red) along with simple Padé (gray) and finite-size (blue) data for $c(T)$ of the $S = 1$ KHAF. Entropy-method curves based on $[4,6](e)$, $[5,5](e)$, $[6,4](e)$, $[5,6](e)$, $[6,5](e)$, $e_0 = -1.41$; simple Padé approximants $[5,6](T)$ and $[6,5](T)$ forming the boundaries of the gray region are shown for $T \geq 0.6$; numerics for $N = 21$ are shown for $T \geq 0.35$. Note that simple Padé approximants and numerics can reproduce the main maximum of $c(T)$ but not a shoulder below it.

This is one of the problems that make it difficult to apply the entropy method to the determination of $\chi(T)$; see Secs. 3.1 and 3.2.

Figures 3, 4, 5, and 6 present our HTE and entropy-method results. The first two figures concern the $S = 1$ case (specific heat and energy gap), whereas the last two ones concern the $S \geq 1$ case (entropy and specific heat).

3. Results and discussion

3.1. $S = 1$

We begin with numerics for finite-size systems with $N = 18$ and $N = 21$, see Figs. 1 and 2. Several observations are immediately evident.

Concerning the energy spectrum shown in Fig. 1, even a quick glance at the three panels of Fig. 1 reveals a distinctive feature of the $S = 1$ case: The ground state which lies in the singlet subspace with $\mathcal{S} = 0$ is gapped and the low-lying excitations in both subspaces with $\mathcal{S} = 0$ and $\mathcal{S} = 1$ have comparable energies; the gap values are: $\Delta_{s-s} \approx 0.497$ and

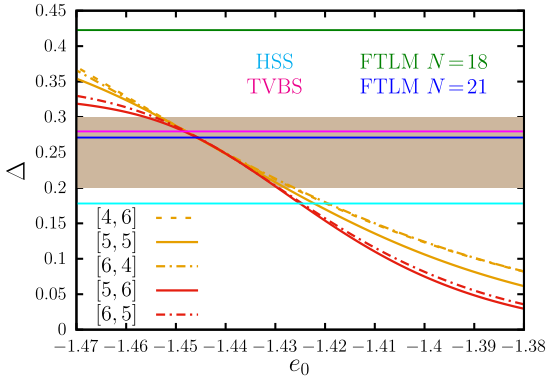


Figure 4. Entropy-method results (orange and red) for the energy gap Δ versus the assumed ground-state energy e_0 of the $S = 1$ KHAF. We also show results for finite systems ($N = 18$ and $N = 21$), of density-matrix renormalization group calculations (gray stripe) [16], as well as results under the hypothesis of hexagonal-singlet solid (HSS) or triangular valence-bond solid (TVBS) ground state [19].

$\Delta_{s-t} \approx 0.423$. Recall, however, that these data refer to finite systems of $N = 18$ sites only. For $N = 21$ we have instead $\Delta_{s-s} \approx 0.271$, and the second exited state is a singlet, too. The smaller gap Δ for $N = 18$ and $N = 21$ is reported in Fig. 4 (colored in green and blue, respectively).

Next, the $S = 1$ results for thermodynamic quantities for different numbers of sites shown in Fig. 2 coincide above the temperature $T/[S(S+1)]$ approximately equals to 0.3 for $s(T)$, 0.4 for $c(T)$, or 0.25 for $\chi(T)$ indicating the confidence region. Since the ground state for both $N = 18$ and $N = 21$ is a singlet, $s(T = 0) = 0$. Additionally, about 52% of the maximum thermal entropy $\ln(2S + 1)$ is realized already at $T/[S(S+1)] = 0.3$. $c(T)$ has a low-temperature maximum, the position of which is size-dependent ($T/[S(S+1)] \approx 0.085$ for $N = 18$ but ≈ 0.055 for $N = 21$) and lies outside the confidence region. $\chi(T)$ illustrates a magnetically gapped spectrum, $\chi(T = 0) = 0$, but the position of the maximum ($T/[S(S+1)] \approx 0.22$ for $N = 18$ and ≈ 0.20 for $N = 21$) is outside the confidence region. Lastly, having only two values $N = 18$ and $N = 21$ it is impossible to predict the low-temperature behavior of c and χ as $N \to \infty$, and thus numerics is inconclusive even for the $S = 1$ case.

Lastly, our $N = 18$ and 21 data agree with the recently obtained

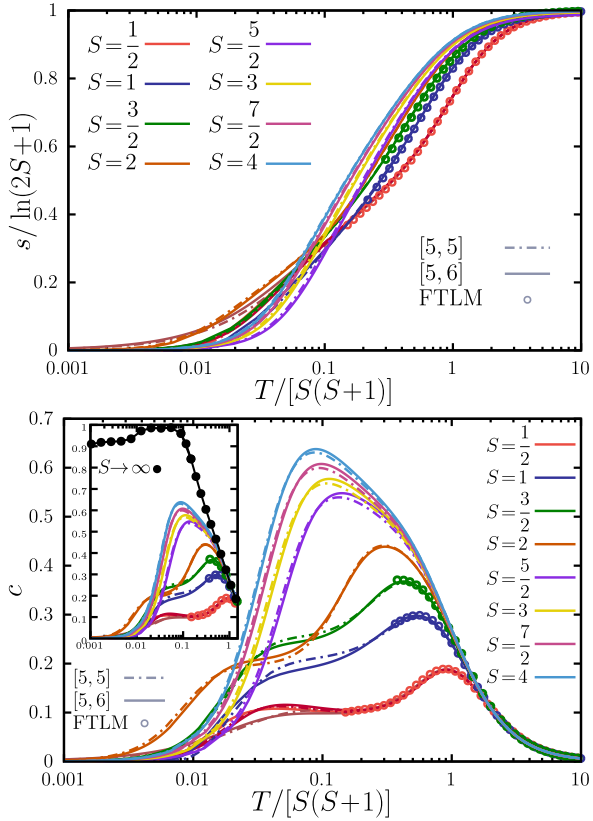


Figure 5. Top and bottom panels: $s(T)$ and $c(T)$ for the spin-S KHAF within the entropy method using Padé approximants $[5,5](e)$ (dash-dotted) and $[5,6](e)$ (solid) only. The values of e_0 are taken from the coupled-cluster method papers [11, 90]. For $S > 1$ the gapless spectrum with $\alpha = 2$ is assumed whereas for $S = 1$ the gapped spectrum is assumed. For $S = 1/2$ the three hues of red correspond to three assumptions: The gapless spectrum with $\alpha = 1, 2$ or the gapped spectrum; on the adopted scale, these curves are quite close to each other. Colored circles correspond to finite-size numerics for $S = 3/2$ ($N = 18$), $S = 1$ ($N = 21$), and $S = 1/2$ ($N = 36$). In the inset, classical Monte Carlo data [91] are shown by black filled circles.

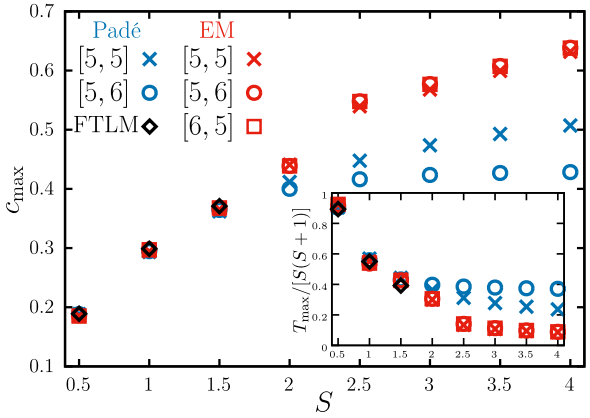


Figure 6. Main maximum of the specific heat $c_{\max} = c(T_{\max})$ for the spin-S KHAF obtained by various methods [entropy method (red), simple Padé approximation (blue), and numerics for $N = 42$, $S = 1/2$ [35], $N = 21$, $S = 1$, and $N = 18$, $S = 3/2$ (black)]. Main panel: $c_{\max}$ versus S. Inset: $T_{\max}/[S(S+1)]$ versus S.

zero-field thermodynamic quantities $c(T)$ and $\chi(T)$ for the $N = 21, 24$, and 27 clusters [23]. However, we believe that the sharp low-temperature peak of $c(T)$, attributed to the formation of a valence-bond crystal state [23], may be a finite-size effect since it shows up outside the confidence region, cf. the sky-blue and blue curves in the middle panel of Fig. 2. Also, the height of the low-temperature peak noticeably decreases as N increases [23].

We pass to the entropy-method calculations, Figs. 3, 4, and 5. As said above, the HTE series up to 11th order (Ref. [88] and Appendix A) for the model at hand is available. Furthermore, the required low-temperature properties are known: We may take for the ground-state energy, e.g., $e_0 = -1.41$, see Appendix A, and postulate gapped excitations. A short comment about the applicability of the entropy method is in order here. The ground-state is not known, but according to existing proposals may possess either broken discrete symmetry (e.g., the simplex valence-bond crystal [14] is a symmetry-breaking state) or not (e.g., the hexagonal-singlet solid [19] is a non-symmetry-breaking state). In the former case, a discrete broken symmetry is restored as temperature increases and passes a phase transition point [23]. Even then, the entropy method, although elaborated for a case without temperature-driven phase transitions, can

provide some evidence of a critical behavior, too, see an example of the Heisenberg model on the bcc lattice in Ref. [70].

In Fig. 3 we report the entropy-method results (along with simple Padé extrapolations and numerics) for $c(T)$ of the $S = 1$ KHAF. As can be seen in this figure, the entropy-method curves agree with simple Padé approximants and numerics in the high-temperature region. Below that, $c(T)$ exhibits a shoulder in the temperature range $T \approx 0.06 - 0.3$. Recall that for the $S = 1/2$ KHAF, the entropy-method calculations under both assumptions, of a gapless spectrum with $c(T) \propto T^{\alpha}$, $\alpha = 1, 2$ as $T \to 0$ [31] or of a gapped spectrum [70], yield an extra low-temperature maximum of $c(T)$ (see also the bottom panel of Fig. 5).

Entropy-method interpolations for $\chi(T)$ (not shown here) provide less favorable outcomes [92]. Thus, assuming as previously $e_0 = -1.41$ and gapped exciations, we found rather poor agreement between various entropy-method curves for $\chi(T)$ [92], especially in comparison to $c(T)$ shown in Fig. 3. To obtain more entropy-method curves $\chi(T)$ which are close to each other, one has to decrease the ground-state energy e_0 from the value -1.41 to the value -1.44; however, such a change of e_0 worsens the predictions for $c(T)$ [92].

To gain more insight into this issue, we discuss the energy gap of the $S = 1$ KHAF. In Fig. 4 we show the dependence of the entropy-method gap Δ as a function of the assumed ground-state energy e_0, see Ref. [69]. Setting $e_0 = -1.41$, we get the gap value within the range $[0.11, 0.15]$. Furthermore, we report in Fig. 4 the singlet-triplet (magnetic or spin) gap according to density-matrix renormalization group calculations, which lies in the range between 0.2 and 0.3 [16] along with the expected gaps for two suggested ground states, hexagon-singlet solid state and triangular valence-bond solid state [19]. As follows from Fig. 4, the entropy-method gap $\Delta = 0.2$ appears if $e_0 \approx -1.43$. It is important to note that the entropy method does not distinguish the singlet-singlet gap Δ_{s-s} and the singlet-triplet gap Δ_{s-t} and yields the value of the smaller energy gap, which governs the low-temperature behavior of the specific heat. Therefore, the entropy method may face a problem if the singlet-singlet (nonmagnetic) gap is smaller than the singlet-triplet gap: The former gap follows from the entropy-method calculations but the latter one, which is larger and not present in the entropy-method scheme, controls the low-temperature behavior of the susceptibility. We may speculate, if for the case under consideration Δ_{s-s} is smaller than Δ_{s-t}, it is not astonishing that the entropy-method output for $\chi(T)$ is worse than for $c(T)$. A decrease of e_0 results in an increase of the energy gap, see Fig. 4, and might improve the entropy-method output for $\chi(T)$. However, the problems with finding $\chi(T)$ within the entropy method may be more intricate as is illustrated for the $S = 1/2$ and $S = 1$ square-lattice Heisenberg antiferromagnets in Ref. [92].

To summarize this subsection, neither numerics nor simple Padé approximants can yield $c(T)$ and $\chi(T)$ below $T = 0.5$. On the other hand, the entropy-method interpolation contains the correct low-temperature behavior of the model at hand and uses $n = 11$ available terms of HTE series. It can predict $c(T)$ for the $S = 1$ KHAF in the whole temperature range, although, in comparison with the $S = 1/2$ case, with a smaller number of almost coinciding $c(T)$ curves. The predictions of the entropy method for $\chi(T)$ are less reliable, which may be related to singlet (nonmagnetic) lowest-energy excitations above the ground state with an energy gap.

3.2. $S > 1$

Now we pass to the cases with $S > 1$ and begin with numerics for finite-size systems. Our FTLM study is restricted to the $S = 3/2$ case. Low-lying energy levels of the $N = 18$ KHAF cluster reported in the right panel of Fig. 1 might agree with the emergence of long-range order as $N \to \infty$, see Refs. [79, 80]. In particular, for each $\mathcal{S} = 0, 1, 2$ subspace, there exist quasi-degenerate joint states around a (dashed) line $E \propto \mathcal{S}(\mathcal{S}+1)$ (in contrast to the $S = 1/2$ case reported in the left panel). Thus, in the subspaces with $\mathcal{S} = 0, 1, 2$ there are sets of 4, 5, 9 levels containing the ground states, and the remaining levels have their energy only about 0.5% higher than the ground-state energy. In the right panel of Fig. 1 the quasi-degenerate joint states in the subspaces with $\mathcal{S} = 0, 1$, and 2 are colored in red, green, and blue, respectively. Thermodynamic quantities $s(T)$, $c(T)$, and $\chi(T)$ presented in Fig. 2 for the $S = 3/2$ KHAF clusters with $N = 15, 18$ exhibit differences in comparison to the $S = 1$ case, however, the most drastic ones occur outside the confidence region. Besides, $\chi(T)$ for $N = 15$ diverges as $T \to 0$ that is obviously related to the (doublet) ground state lying in the subspace $\mathcal{S} = 1/2$.

Next we turn to the entropy-method calculations. Since the ground state for $S \geq 3/2$ likely possesses a magnetic long-range order, it is reasonable to assume a gapless spectrum and a quadratically vanishing specific heat $c(T) \propto T^2$ as $T \to 0$ for all $S \geq 3/2$. The values of e_0 are available from the coupled cluster method calculations [11]. Although the values of χ_0 may be taken, in principle, from the rotation-invariant Green's-function method calculations [64], but in view of that (i) the latter approach is not precise enough and (ii) the entropy method faces some difficulties in obtaining $\chi(T)$ for gapples excitations too [92], we

restrict ourselves in what follows to the specific heat $c(T)$. Before presenting our findings, it might be worth to recall that (i) $S = 3/2$ results were reported in Ref. [24] (but the curve $c(T)$ reported there hardly obeys the sum rule $\int_0^\infty \mathrm{d}T c(T)/T = \ln(2S+1)$, see Fig. 4 in Ref. [92]) and (ii) a number of reliable classical Monte Carlo simulations data for $c(T)$ and $\chi(T)$ for the case $S \to \infty$ were reported in Refs. [25, 39, 40, 91, 93]. The specific heat for the classical KHAF is shown in the inset in Fig. 5 by black filled circles.

In the following, we examined in some detail the entropy-method curves $c(T)$ for $S = 3/2$, $S = 2$, and $S = 5/2$ using Padé approximants $[u, d](e)$ to the 9th, 10th, and 11th orders series for the auxiliary function $G(e)$, see Sec. 2.2 and Ref. [92]. Below, we report as representative instances the 10th and 11th order Padé approximants $[5, 5](e)$ and $[5, 6](e)$. As is evident from Figs. 5 and 6, the predictions based on $[5, 5](e)$ and $[5, 6](e)$ are in reasonably good agreement with each other. In the top and bottom panels of Fig. 5 we report $s(T)$ and $c(T)$ for several spin values up to $S = 4$ to demonstrate how the pure quantum case ($S = 1/2$) transforms into the classical one ($S \to \infty$) as S grows. The upper panel of this figure shows how the entropy increases as temperature grows. For high temperatures, the entropy s versus temperature $T/[S(S+1)]$ varies monotonously with growing S in contrast to low temperatures, where the pattern is rather intricate. This is in alignment with the temperature profiles of the specific heat $c(T) = T\partial s(T)/\partial T$ shown in the bottom panel of Fig. 5. As can be seen from this panel, for $S = 1/2$, 1, 3/2 there are some low-temperature features (peak or shoulder) in the curves c versus $T/[S(S+1)]$ in addition to the main peak; the case $S = 2$ is marginal; and for $S = 5/2$, 3, 7/2, 4 there is only one main peak in the curves of the specific heat c versus temperature $T/[S(S+1)]$.

Moreover, in Fig. 6 we illustrate how the main peak in the specific heat $c_{\max} = c(T_{\max})$ is modified as S varies. Namely, we report the dependence of the height of the main maximum $c_{\max}$ (main panel) and its position $T_{\max}$ (inset) as functions of the spin value S. Besides the entropy method outcomes of $c_{\max}$ and $T_{\max}$ (colored in red), we show the simple Padé approximations (colored in blue), and numerics for $S =$ 1/2, 1, 3/2 (colored in black). Again the spin value $S = 2$ is a special one. As is seen in the inset, the position of the main peak $T_{\max}$ moves to lower $T/[S(S+1)]$ as S increases from 1/2 to 2 and all methods yield almost identical predictions for that. When S grows beyond 2, the main peak position $T_{\max}$ continues to decrease, however, the predictions from different methods are scattered. Similar trends occur for the main peak height of the specific heat $c(T_{\max})$, see the main panel.

In summary, according to the entropy method, an extra low-temperature feature below the main maximum of $c(T)$ is present for $S = 1/2$, 1, 3/2, but not for the larger spin values $S > 2$. Some observed features are similar to those obtained by simple Padé approximations to HTE series [88] and the rotation-invariant Green's-function method calculations [64] of $c(T)$ for the spin-S KHAF. For example, according to Refs. [64, 88], the position of the main maximum of $c(T)$ shifts towards lower values of $T/[S(S+1)]$ with increasing S, however, the role of low-lying excitations relevant for the low-temperature physics is beyond those approaches. It is also instructive to compare Figs. 5 and 6 to the corresponding results obtained using entropy-method interpolation, simple Padé approximants, and quantum Monte Carlo simulations for the spin-S square-lattice Heisenberg antiferromagnet (see Figs. 7 and 8 in Appendix B). For the square-lattice case, $s(T)$ and $c(T)$ curves vary very regularly as S grows; for more details see Appendix B.

4. Summary

The main challenge in describing the thermodynamics of the spin-S KHAF is a lack of appropriate methods for the calculation of thermodynamic quantities for the whole temperature range. In the present paper, we use finite-size numerics restricted to $S = 1, 3/2$ and HTE series up to 11th order augmented by the entropy-method interpolation to obtain thermodynamic quantities of the spin-S KHAF. While the numerics yields results free of finite-size effects only at moderate and high temperatures, the entropy-method data linking low- and high-temperature regions yields thermodynamics over the full temperature range. The presented finite-temperature results may provide benchmark data for measurements in spin-S KHAF materials. Our findings for the specific heat $c(T)$ of the spin-S KHAF presented in the bottom panel of Fig. 5 illustrate a crossover between pure quantum ($S = 1/2$) and classical ($S \to \infty$) behavior. In particular, the characteristic shoulder of $c(T)$ that occurs at low temperatures for $S = 1/2$ disappears when $S > 2$.

It is worth mentioning here a recent theory of a hidden energy scale in geometrically frustrated magnets suggested in Refs. [94–97]. The hidden energy scale, which is significantly lower than the microscopic energy scale of spin interactions, manifests itself as a lower-temperature peak, well below the common (main) higher-temperature peak, in $c(T)$ [94, 95, 98]. With our study we may put forward a question about the role of the spin value S in the hidden energy scale scenario for geometrically

frustrated magnets.

Acknowledgments

We commemorate our co-author Johannes Richter, who passed untimely and who had initiated this research. O. D. acknowledges the kind hospitality of the MPIPKS, Dresden in September-November of 2019 when this study was launched. The authors would also like to acknowledge their collaboration with A. Hauser and P. Müller during the early stages of the study. This project is funded by the National Research Foundation of Ukraine (2023.03/0063, Frustrated quantum magnets under various external conditions). O. D. thanks A. Honecker, J. Strečka, and K. Karlová for kind hospitality at the COOLMAG2025 Workshop Magnetic Cooling and Frustrated Magnetism, October 27th – 29th, 2025, Košice, Slovakia, and S. Capponi for valuable discussions. T. H., T. K., and O. D. are thankful to the Armed Forces of Ukraine for protection since 2014, and especially since February 24, 2022.

A. Reference materials: e_0 and high-temperature series for $S \geq 1$

In Table 1 and Table 2 we collected the ground-state energies obtained by various authors for the case $S = 1$ and $S = 3/2$, respectively. The coupled-cluster method ground-state energy can be found in Table 1 of Ref. [90].

Concerning the opposite limit of infinite temperature, HTE up to 10th order for arbitrary spin S can be found in Appendix B of Ref. [88]. Here, we report the 11th order coefficients in HTE for the KHAF with $S = 1$, 3/2, 2, 5/2, 3, 7/2, 4. We have

$$d_{11}=-\frac{76\,377\,321\,757}{66\,134\,880}J^{11},$$
$$c_{11}=\frac{49\,904\,041}{47\,239\,200}J^{10} \tag{A1}$$

for $S = 1$,

$$d_{11}=-\frac{6\,245\,386\,099\,381}{24\,772\,608}J^{11},$$
$$c_{11}=\frac{12\,298\,193\,957}{2\,211\,840}J^{10} \tag{A2}$$

Table 1. The ground-state energy per site e_0 for the $S = 1$ KHAF obtained by various methods [exact diagonalization (ED) for various clusters of $N = 18$ sites and $N = 24$, series expansion (SE) method assuming $\sqrt{3}\times\sqrt{3}$ or q=0 order, nonperturbative linked-cluster expansion (NLCE), density-matrix renormalization group (DMRG) algorithm, tensor-network (TN) methods, coupled-cluster method (CCM) assuming $\sqrt{3}\times\sqrt{3}$ or q=0 order, hexagonal singlet solid (HSS) state, resonating Affleck-Kennedy-Lieb-Tasaki loop (RAL) state, triangular valence-bond solid (TVBS) state].

	e_0/S^2 $(S=1)$
ED	$-1.451\,10$ (N=18a), $-1.439\,26$ (N=18b) [16]; $-1.426\,689\,4$ (N=24) [17]
SE	$-1.395\,0$ ($\sqrt{3}\times\sqrt{3}$), $-1.390\,3$ (q=0) [21]
NLCE	$-1.411\,4$ [20]
DMRG	$-1.410(2)$ [16]; $-1.411\,1$, $-1.412\,2$ [19]
TN	$-1.411\,6(4)$ [14]
CCM	$-1.403\,1$ ($\sqrt{3}\times\sqrt{3}$), $-1.396\,5$ (q=0) [11]
HSS	-1.36 [16]; $-1.360\,0$ [18]; $-1.410\,95$ [19]
RAL	-1.383 [12]
TVBS	$-1.387\,1$ [18]; $-1.391\,2 \pm 0.002\,5$ [19]; -1.40 [21]

Table 2. The ground-state energy per site e_0 for the $S = 3/2$ KHAF obtained by various methods [series expansion (SE) method, tensor-network (TN) methods, coupled-cluster method (CCM)].

	e_0/S^2 $(S=3/2)$
SE	-1.2530 ($\sqrt{3}\times\sqrt{3}$), -1.2527 (q=0) [21]
TN	$-1.265(2)$ [24]
CCM	-1.2680 ($\sqrt{3}\times\sqrt{3}$), -1.2643 (q=0) [11]

for $S = 3/2$,

$$d_{11} = -\frac{625\,587\,268\,339}{151\,200} J^{11},$$
$$c_{11} = \frac{2\,863\,397\,370\,551}{1\,260\,000} J^{10} \tag{A3}$$

for $S = 2$,

$$d_{11} = \frac{10\,417\,179\,602\,755\,425\,863}{15\,479\,341\,056} J^{11},$$
$$c_{11} = \frac{17\,166\,356\,000\,458\,470\,419}{77\,396\,705\,280} J^{10} \tag{A4}$$

for $S = 5/2$,

$$d_{11} = \frac{90\,425\,361\,936\,437}{2\,520} J^{11},$$
$$c_{11} = \frac{7\,229\,967\,967\,257\,239}{793\,800} J^{10} \tag{A5}$$

for $S = 3$,

$$d_{11} = \frac{1\,708\,825\,945\,895\,179\,243}{1\,966\,080} J^{11},$$
$$c_{11} = \frac{3\,104\,351\,513\,640\,540\,433}{14\,745\,600} J^{10} \tag{A6}$$

for $S = 7/2$, and

$$d_{11} = \frac{44\,103\,941\,566\,868\,273\,233}{3\,306\,744} J^{11},$$
$$c_{11} = \frac{53\,216\,684\,483\,872\,733\,269}{16\,533\,720} J^{10} \tag{A7}$$

for $S = 4$.

B. Entropy-method results for the spin-S Heisenberg antiferromagnet on the square lattice

In this appendix, we illustrate applying the entropy-method interpolation to the spin-S square-lattice Heisenberg antiferromagnet – a nonfrustrated lattice but with the same coordination number 4 as the kagome lattice. We generate HTE series up to 10th order using the Magdeburg code [87, 88], take the values of e_0 from Ref. [90], and set the exponent

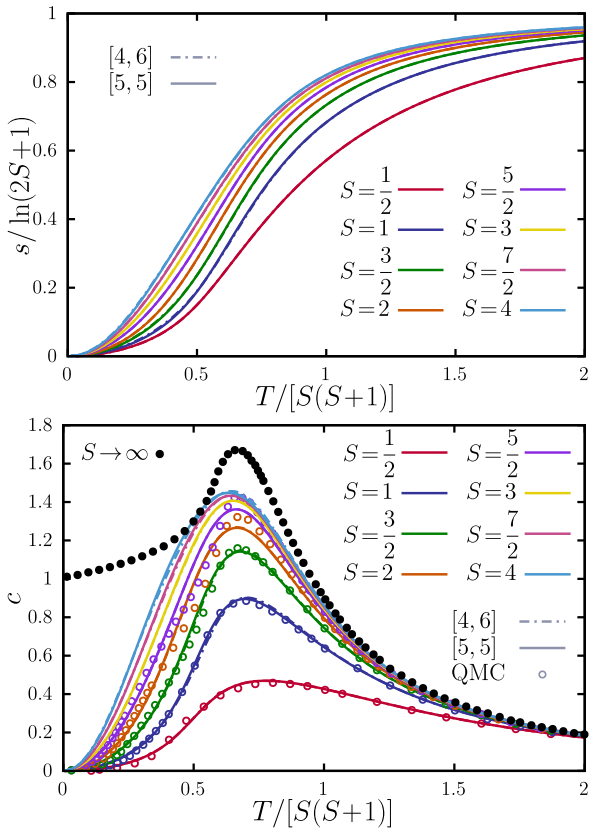


Figure 7. Top and bottom panels: $s(T)$ and $c(T)$ for the spin-S square-lattice Heisenberg antiferromagnet within the entropy method (colored lines) and quantum Monte Carlo (colored circles) [99]. Classical Monte Carlo data are shown by black filled circles. This figure has to be compared to Fig. 5.

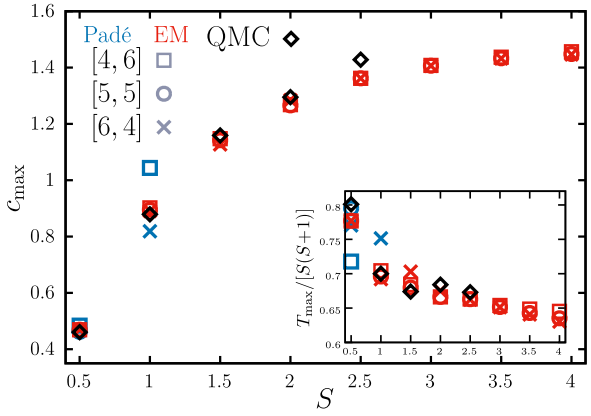


Figure 8. Main maximum of the specific heat $c_{\max} = c(T_{\max})$ for the spin-S square-lattice Heisenberg antiferromagnet obtained by various methods [entropy method (red), simple Padé approximation (blue), and quantum Monte Carlo (black)]. Main panel: $c_{\max}$ versus S. Inset: $T_{\max}/[S(S+1)]$ versus S. This figure has to be compared to Fig. 6.

for power-law specific heat decay as $T \to 0$ to $\alpha = 2$. In Figs. 7 and 8 we present the results similar the ones in Figs. 5 and 6, but now for the spin-S square-lattice Heisenberg antiferromagnet. Besides, we report quantum Monte Carlo simulations data for S up to 5/2 (colored circles) [99]: They agree reasonably well with the entropy-method predictions.

Comparing Figs. 7 and 5, one immediately concludes that both $s(T)$ and $c(T)$ curves for the square-lattice case vary very regularly with increasing the spin value S. At $T/[S(S+1)] = 0.3$ only 18% of the maximum thermal entropy $\ln(2S+1)$ is realized even for $S = 4$ (and less than 5.6% for $S = 1$). The specific heat curves $c(T)$ has always one maximum; the position of this maximum $T_{\max}$ and its height $c_{\max} = c(T_{\max})$ are predicted consistently by various methods, cf. Figs. 8 and 6. It is noteworthy to mention that simple Padé approximants to HTE series fail to catch the main maximum as $S > 1$; therefore, the simple Pade approximations colored in blue in Fig. 8 refer to $S = 1/2$ and $S = 1$ only. Note also that the peak height $c_{\max}$ is about 2 times higher and occurs at somewhat higher temperatures. Besides, $c(T)$ for $S = 4$ is already quite close to such a curve for the classical spin value $S \to \infty$.

References

1. C. Lacroix, P. Mendels, and F. Mila, *Introduction to Frustrated Magnetism: Materials, Experiments, Theory*, Springer Series in Solid-State Sciences (Springer Berlin Heidelberg, 2011).
2. J. Khatua, B. Sana, A. Zorko, M. Gomilšek, K. Sethupathi, M. R. Rao, M. Baenitz, B. Schmidt, and P. Khuntia, Physics Reports **1041**, 1 (2023).
3. Z. Y. Meng, C. D. Batista, and S. Li, Nature Physics (2026).
4. S. Yan, D. A. Huse, and S. R. White, Science **332**, 1173 (2011).
5. S. Depenbrock, I. P. McCulloch, and U. Schollwöck, Phys. Rev. Lett. **109**, 067201 (2012).
6. Y. Iqbal, F. Becca, S. Sorella, and D. Poilblanc, Phys. Rev. B **87**, 060405(R) (2013).
7. Y.-C. He, M. P. Zaletel, M. Oshikawa, and F. Pollmann, Phys. Rev. X **7**, 031020 (2017).
8. K. Hida, Journal of the Physical Society of Japan **69**, 4003 (2000).
9. K. Hida, Journal of the Physical Society of Japan **70**, 3673 (2001).
10. Z. Cai, S. Chen, and Y. Wang, Journal of Physics: Condensed Matter **21**, 456009 (2009).
11. O. Götze, D. J. J. Farnell, R. F. Bishop, P. H. Y. Li, and J. Richter, Phys. Rev. B **84**, 224428 (2011).
12. W. Li, S. Yang, M. Cheng, Z.-X. Liu, and H.-H. Tu, Phys. Rev. B **89**, 174411 (2014).
13. T. Picot and D. Poilblanc, Phys. Rev. B **91**, 064415 (2015).
14. T. Liu, W. Li, A. Weichselbaum, J. von Delft, and G. Su, Phys. Rev. B **91**, 060403 (2015).
15. O. Götze and J. Richter, Phys. Rev. B **91**, 104402 (2015).
16. H. J. Changlani and A. M. Läuchli, Phys. Rev. B **91**, 100407 (2015).
17. H. Nakano and T. Sakai, Journal of the Physical Society of Japan **84**, 063705 (2015).
18. W. Li, A. Weichselbaum, J. von Delft, and H.-H. Tu, Phys. Rev. B **91**, 224414 (2015).
19. S. Nishimoto and M. Nakamura, Phys. Rev. B **92**, 140412 (2015).
20. D. Ixert, T. Tischler, and K. P. Schmidt, Phys. Rev. B **92**, 174422 (2015).
21. J. Oitmaa and R. R. P. Singh, Phys. Rev. B **93**, 014424 (2016).
22. T. Picot, M. Ziegler, R. Orús, and D. Poilblanc, Phys. Rev. B **93**, 060407 (2016).
23. K. Morita, Quantum magnetism of the spin-1 kagome-lattice antiferromagnet (2026), arXiv:2607.03086 [cond-mat.str-el] .

24. T. Liu, W. Li, and G. Su, Phys. Rev. E **94**, 032114 (2016).
25. J. T. Chalker, P. C. W. Holdsworth, and E. F. Shender, Phys. Rev. Lett. **68**, 855 (1992).
26. H.-J. Schmidt, Theory of ground states for classical Heisenberg spin systems II (2017), arXiv:1707.02859 [cond-mat.other] .
27. N. Elstner and A. P. Young, Phys. Rev. B **50**, 6871 (1994).
28. T. Nakamura and S. Miyashita, Phys. Rev. B **52**, 9174 (1995).
29. P. Tomczak and J. Richter, Phys. Rev. B **54**, 9004 (1996).
30. P. Sindzingre, G. Misguich, C. Lhuillier, B. Bernu, L. Pierre, C. Waldtmann, and H.-U. Everts, Phys. Rev. Lett. **84**, 2953 (2000).
31. G. Misguich and B. Bernu, Phys. Rev. B **71**, 014417 (2005).
32. M. Rigol, T. Bryant, and R. R. P. Singh, Phys. Rev. Lett. **97**, 187202 (2006).
33. M. Rigol, T. Bryant, and R. R. P. Singh, Phys. Rev. E **75**, 061118 (2007).
34. T. Shimokawa and H. Kawamura, Journal of the Physical Society of Japan **85**, 113702 (2016).
35. J. Schnack, J. Schulenburg, and J. Richter, Phys. Rev. B **98**, 094423 (2018).
36. X. Chen, S.-J. Ran, T. Liu, C. Peng, Y.-Z. Huang, and G. Su, Science Bulletin **63**, 1545 (2018).
37. B. Bernu, L. Pierre, K. Essafi, and L. Messio, Phys. Rev. B **101**, 140403 (2020).
38. C. Hotta and K. Asano, Phys. Rev. B **98**, 140405 (2018).
39. A. J. García-Adeva and D. L. Huber, Phys. Rev. B **63**, 140404 (2001).
40. M. E. Zhitomirsky, Phys. Rev. Lett. **88**, 057204 (2002).
41. M. R. Norman, Rev. Mod. Phys. **88**, 041002 (2016).
42. P. Mendels and F. Bert, Comptes Rendus. Physique **17**, 455 (2016).
43. Q. Barthélemy, A. Demuer, C. Marcenat, T. Klein, B. Bernu, L. Messio, M. Velázquez, E. Kermarrec, F. Bert, and P. Mendels, Phys. Rev. X **12**, 011014 (2022).
44. F. Ferrari, S. Niu, J. Hasik, Y. Iqbal, D. Poilblanc, and F. Becca, SciPost Phys. **14**, 139 (2023).
45. F. Heully-Alary, N. Ben Amor, N. Suaud, L. Messio, C. de Graaf, and N. Guihéry, SciPost Phys. Core **8**, 092 (2025).
46. S. Jiang, A. C. Campello, W. He, J. Wen, D. M. Pajerowski, Y. S. Lee, and H.-C. Jiang, npj Computational Materials **12**, 91 (2026).
47. K. Awaga, T. Okuno, A. Yamaguchi, M. Hasegawa, T. Inabe, Y. Maruyama, and N. Wada, Phys. Rev. B **49**, 3975 (1994).
48. N. Wada, T. Kobayashi, H. Yano, T. Okuno, A. Yamaguchi, and K. Awaga, J. Phys. Soc. Jpn. **66**, 961 (1997).
49. I. Watanabe, N. Wada, H. Yano, T. Okuno, K. Awaga, S. Ohira, K. Nishiyama, and K. Nagamine, Phys. Rev. B **58**, 2438 (1998).
50. D. Papoutsakis, D. Grohol, and D. G. Nocera, Journal of the American Chemical Society **124**, 2647 (2002).
51. G. Lawes, M. Kenzelmann, N. Rogado, K. H. Kim, G. A. Jorge, R. J. Cava, A. Aharony, O. Entin-Wohlman, A. B. Harris, T. Yildirim, Q. Z. Huang, S. Park, C. Broholm, and A. P. Ramirez, Phys. Rev. Lett. **93**, 247201 (2004).
52. J. N. Behera and C. N. R. Rao, Journal of the American Chemical Society **128**, 9334 (2006).
53. T. Matsushita, N. Hamaguchi, K. Shimizu, N. Wada, W. Fujita, K. Awaga, A. Yamaguchi, and H. Ishimoto, Journal of the Physical Society of Japan **79**, 093701 (2010).
54. W. Miiller, M. Christensen, A. Khan, N. Sharma, R. B. Macquart, M. Avdeev, G. J. McIntyre, R. O. Piltz, and C. D. Ling, Chemistry of Materials **23**, 1315 (2011).
55. D. E. Freedman, R. Chisnell, T. M. McQueen, Y. S. Lee, C. Payen, and D. G. Nocera, Chem. Commun. **48**, 64 (2012).
56. S. Hara, H. Sato, and Y. Narumi, Journal of the Physical Society of Japan **81**, 073707 (2012).
57. E. T. Connolly, P. Reeves, D. Boldrin, and A. S. Wills, Journal of Physics: Condensed Matter **30**, 025801 (2017).
58. H. J. Silverstein, R. Sinclair, A. Sharma, Y. Qiu, I. Heinmaa, A. Leitmäe, C. R. Wiebe, R. Stern, and H. Zhou, Phys. Rev. Mater. **2**, 044006 (2018).
59. I. S. Hagemann, Q. Huang, X. P. A. Gao, A. P. Ramirez, and R. J. Cava, Phys. Rev. Lett. **86**, 894 (2001).
60. D. Bono, P. Mendels, G. Collin, N. Blanchard, F. Bert, A. Amato, C. Baines, and A. D. Hillier, Phys. Rev. Lett. **93**, 187201 (2004).
61. B. Fåk, F. C. Coomer, A. Harrison, D. Visser, and M. E. Zhitomirsky, Europhysics Letters **81**, 17006 (2007).
62. K. Okuta, S. Hara, H. Sato, Y. Narumi, and K. Kindo, Journal of the Physical Society of Japan **80**, 063703 (2011).
63. S. Okubo, R. Nakata, S. Ikeda, N. Takahashi, T. Sakurai, W.-M. Zhang, H. Ohta, T. Shimokawa, T. Sakai, K. Okuta, S. Hara, and H. Sato, Journal of the Physical Society of Japan **86**, 024703 (2017).
64. P. Müller, A. Zander, and J. Richter, Phys. Rev. B **98**, 024414 (2018).
65. P. Ghosh, T. Müller, Y. Iqbal, R. Thomale, and H. O. Jeschke, Phys. Rev. B **110**, 094406 (2024).
66. D. Yaremchuk, T. Hutak, V. Baliha, T. Krokhmalskii, O. Derzhko,

J. Schnack, and J. Richter, Phys. Rev. B **112**, 024402 (2025).
67. A. M. Läuchli, J. Sudan, and E. S. Sørensen, Phys. Rev. B **83**, 212401 (2011).
68. A. M. Läuchli, J. Sudan, and R. Moessner, Phys. Rev. B **100**, 155142 (2019).
69. B. Bernu and G. Misguich, Phys. Rev. B **63**, 134409 (2001).
70. B. Bernu and C. Lhuillier, Phys. Rev. Lett. **114**, 057201 (2015).
71. O. Derzhko, T. Hutak, T. Krokhmalskii, J. Schnack, and J. Richter, Phys. Rev. B **101**, 174426 (2020).
72. V. Grison, P. Viot, B. Bernu, and L. Messio, Phys. Rev. B **102**, 214424 (2020).
73. M. G. Gonzalez, B. Bernu, L. Pierre, and L. Messio, SciPost Phys. **12**, 112 (2022).
74. T. Hutak, T. Krokhmalskii, O. Derzhko, and J. Richter, The European Physical Journal B **96**, 50 (2023).
75. T. Hutak, T. Krokhmalskii, J. Schnack, J. Richter, and O. Derzhko, Phys. Rev. B **110**, 054428 (2024).
76. T. Hutak, Phys. Rev. B **112**, 104405 (2025).
77. J. Jaklič and P. Prelovšek, Phys. Rev. B **49**, 5065(R) (1994).
78. P. W. Anderson, Phys. Rev. **86**, 694 (1952).
79. C. Lhuillier, P. Sindzingre, and J. B. Fouet, Canadian Journal of Physics **79**, 1525 (2001).
80. B. Bernu, C. Lhuillier, and L. Pierre, Phys. Rev. Lett. **69**, 2590 (1992).
81. B. Bernu, C. Lhuillier, and L. Pierre, Journal of Low Temperature Physics **89**, 523 (1992).
82. B. Bernu, P. Lecheminant, C. Lhuillier, and L. Pierre, Phys. Rev. B **50**, 10048 (1994).
83. P. Lecheminant, B. Bernu, C. Lhuillier, and L. Pierre, Phys. Rev. B **52**, 6647 (1995).
84. B. Bernu, P. Lecheminant, C. Lhuillier, and L. Pierre, Physica Scripta **1993**, 192 (1993).
85. P. Lecheminant, B. Bernu, C. Lhuillier, L. Pierre, and P. Sindzingre, Phys. Rev. B **56**, 2521 (1997).
86. C. Waldtmann, H.-U. Everts, B. Bernu, C. Lhuillier, P. Sindzingre, P. Lecheminant, and L. Pierre, Eur. Phys. J. B **2**, 501 (1998).
87. H.-J. Schmidt, A. Lohmann, and J. Richter, Phys. Rev. B **84**, 104443 (2011).
88. A. Lohmann, H.-J. Schmidt, and J. Richter, Phys. Rev. B **89**, 014415 (2014).
89. L. Pierre, B. Bernu, and L. Messio, SciPost Phys. **17**, 105 (2024).

90. D. J. J. Farnell, O. Götze, J. Schulenburg, R. Zinke, R. F. Bishop, and P. H. Y. Li, Phys. Rev. B **98**, 224402 (2018).
91. C. M. Gembé, *Frustrated Magnetism, Monopole Dynamics, and Non-Coplanar Ordering in Classical Spin Systems. Insights from Monte Carlo Simulations*, Ph.D. thesis, University of Cologne (2023).
92. T. Hutak, J. Richter, T. Krokhmalskii, and O. Derzhko, Preliminaries on thermodynamics of the spin-S Heisenberg antiferromagnet on the kagome lattice (2024), Institute for Condensed Matter Physics of the National Academy of Sciences of Ukraine, ICMP-24-04E .
93. M. E. Zhitomirsky, Phys. Rev. B **78**, 094423 (2008).
94. P. Popp, A. P. Ramirez, and S. Syzranov, Phys. Rev. Lett. **134**, 226701 (2025).
95. A. P. Ramirez and S. V. Syzranov, Materials Advances **6**, 1213 (2025).
96. S. Zhu, A. P. Ramirez, and S. Syzranov, Low-temperature entropies and possible states in geometrically frustrated magnets (2025), arXiv:2511.02899 [cond-mat.str-el] .
97. P. Popp, S. Rosenkranz, A. P. Ramirez, and S. Syzranov, Spin correlations, low-energy scales, and anisotropy scaling in kagome frustrated magnets (2026), arXiv:2606.12512 [cond-mat.str-el] .
98. T. Krokhmalskii, T. Hutak, and O. Derzhko, Condensed Matter Physics **28**, 43502 (2025).
99. D. C. Johnston, R. J. McQueeney, B. Lake, A. Honecker, M. E. Zhitomirsky, R. Nath, Y. Furukawa, V. P. Antropov, and Y. Singh, Phys. Rev. B **84**, 094445 (2011).